 doi:10.20944/preprints202011.0347.v1

Article

Mapping the Melatonin Suppression, Star Light and Induced Photosynthesis Indices with the LANcube

Martin Aubé [1,2,3,†,*], Charles Marseille [2], Amar Farkouh [1] Adam Dufour [1], Alexandre Simoneau [2], Jaime Zamorano [4,5], Johanne Roby [1], and Carlos Tapia [4]

1 Cégep de Sherbrooke
2 Département de géomatique appliquée, Université de Sherbrooke
3 Physics department, Bishop's University
4 Dept. Física de la Tierra y Astrofísica, Universidad Complutense de Madrid
5 Instituto de Física de Partículas y del Cosmos (IPARCOS), Universidad Complutense de Madrid
* Correspondence: martin.aube@cegepsherbrooke.qc.ca; Tel.: 1-819-564-6350 #4146
† Current address: 475 rue du Cégep, Sherbrooke, Québec, Canada J1E 4K1

Abstract: Increased exposure to artificial light at night can affect human health including disruption of melatonin production and circadian rhythms and extend to increased risks of hormonal cancers and other serious diseases. In addition, multiple negative impacts on fauna and flora are well documented, and it is a matter of fact that artificial light at night is a nuisance for ground-based astronomy. These impacts are frequently linked to the colour of the light or more specifically to its spectral content. Artificial light at night is often mapped by using space borne sensors, but most of them are panchromatic and thus insensitive to the colour. In this paper, we suggest a method that allows high resolution mapping of the Artificial light at night by using ground-based measurements with the LANcube system. The device separates the light detected in four bands (Red, Green, Blue, and Clear) and provides this information for six faces of a cube. We found relationships between the LANcube's colour ratios and 1- the Melatonin Suppression Index, 2- the StarLight Index and 3- the Induced Photosynthesis Index. We show how such relationships combined with data acquisition from a LANcube positioned on the top of a car can be used to produce spectral indices maps of a whole city in a few hours.

Keywords: Artificial Light at Night; Intrusive Light ; Direct Light Pollution ; Radiometry ; Multispectral ; Multiangular ; Melatonin Suppression Index ; Star Light Index ; Spectroscopy ; Measurement ; Synthetic photometry

1. Introduction

For several decades, the increase of artificial light at night (ALAN) has greatly altered the nocturnal integrity in which living organisms evolve, both diurnal and nocturnal. ALAN contributes to the disruption of daily, lunar and seasonal cycles of natural light [1] and has significant consequences on fauna [1,2], on flora [3], on the starry sky [4] and on human health [5].

It is well known that day/night light cycles regulate circadian rhythms and synchronize the circadian clock in humans [6]. Light has also been shown to impact several physiological functions such as melatonin suppression [7]. Indeed, melatonin is a hormone produced by the pineal gland in relation to the light detected by a non-visual retina photoreceptor, the melanopsin. This photoreceptor has a maximum spectral sensitivity at blue wavelengths [8,9]. There is strong evidence that many biological effects of artificial light at night (ALAN) are directly related to its spectral content. For example, some studies have shown that exposure to blue-enriched light may increase the risk of hormone-dependent cancers [10–12]. One accurate way to detect the impact of ALAN on circadian systems is to monitor the level of melatonin in biofluids, but such a procedure can be complex to perform on large samples and/or large areas.

 doi:10.20944/preprints202011.0347.v1

In 2013, Aubé *et al.* [13] proposed the Melatonin Suppression Index (MSI) as a new metric to evaluate the potential effect of the spectral distribution of the light on the melatonin suppression mechanism. The MSI only requires the knowledge of the ambient spectral content of ALAN to be determined. This index was designed to disentangle the effect associated with the colour of spectral content from the one related to the absolute visual light level. The MSI is typically ranging on a scale from 0 to ≈1, 0 being a spectrum with no impact on melatonin suppression and 1 being the impact of the sunlight spectrum. The sun spectrum (actually the Commission Internationale de l'Éclairage (CIE) standard illuminant D65) was taken as a reference in the calculation of this index because the sun is the main natural source of light under which the human body adapted over time. It contains the whole visible part of the light spectrum. The MSI uses a fit of the Melatonin Suppression Action Spectrum (MSAS) data acquired by Thapan *et al.* [14] and Brainard *et al.* [9] as a weighting function. The MSI is mostly affected by blue-enriched light due to the high sensitivity of the melanopsin to this spectral range [15]. Lamps with a larger percentage of blue light than the sun light can have a MSI higher than 1 even if it is not common in typical lighting technologies. Garcia-Saenz *et al.* [10] and Garcia-Saenz *et al.* [11] used the MSI as a proxy for the blue light content effect on breast, prostate and colorectal cancers in Madrid and Barcelona. They found correlations between the MSI from street lights nearby homes of participants to the MCC-Spain epidemiological study for the three cancers evaluated.

In a similar way to the MSI, the Star Light Index (SLI, [13]) can be used to monitor the impact of the spectrum of ALAN on stellar observations. The threat to astronomical observation capacities is caused by the scattering of ALAN by molecules and aerosols in the atmosphere. The light travelling upward can then be redirected to an observer and hence compete with the low light levels coming from astronomical objects. The SLI. T also typically spans from 0 to ≈1, 0 being a colour that does not compete with stars visibility and 1 being a colour that affects star visibility like a D65 spectrum would do. The SLI uses the scotopic sensitivity as a weighting function. Blue-enriched light has also revealed to give higher SLI values, because that the SLI is more sensitive in the blue region.

Finally, the Induced Photosynthesis Index (IPI, [13]) can be used to monitor the impacts of the spectrum of artificial lights on plants. As for the MSI and the SLI, the IPI typically spans from 0 to ≈1, 0 being a colour that does not stimulate the photosynthesis process and 1 being a colour that affects photosynthesis like a D65 spectrum would do. The IPI uses the Photosynthesis Action Spectrum (PAS, DIN5031–10 [16]) as a weighting function.

The calculation of the MSI, the SLI and the IPI for a given light radiant flux depends on the shape of its spectral power distribution. This calculation requires the use of a spectrometer to sample the lamp spectrum. However, spectral measurements are not the easiest to obtain, especially if many of them are required. It has been shown that three bands Red, Green, Blue (RGB) photometric data can be used to determine spectral indices or photoreceptor stimuli from values recorded by a Digital single-lens reflex camera (DSLR) [17,18]. That method is much faster and easier to perform.

In this paper, we developed a similar method of calculating the MSI, the SLI and the IPI out of four bands RGB and Clear (RGBC) photometric data detected by the LANcube system. This method relies on a cross calibration between RGBC values of the LANcube obtained using synthetic photometry method applied on a large spectral database along with the MSI, the SLI, the IPI determination by the integration of the same spectra.

2. Materials and Methods

In this section, we explain how the raw RGBC values of the LANcube can be converted into the MSI, the SLI, and the IPI after determining relationships between colour-colour ratios and each index.

2.1. The LANcube system

The LANcube aka LAN^3 is a new device developed by Pr. Aubé's research group. It is intended to sample the multispectral and multidirectional properties of the Direct Artificial Light At Night (DALAN) into any environment (indoor or outdoor). It was designed to allow the evaluation of the

 doi:10.20944/preprints202011.0347.v1

impact of DALAN on human health and ecosystems. The LAN^3 is a cube-shaped device having a sensor with four visible spectral bands (red, green, blue and clear) on each of its six faces. The respective spectral sensitivity of each band is shown in Figure 1a. The sensor used is the TCS 34725 colour sensor manufactured by Texas Advanced Optoelectronic Solutions Inc. (TAOS). A Cole-Parmer watch glass protects the sensor electronics from the outside world. The spectral response of each band of the sensor including the effect of the spectral transmittance of the watch glass was determined at the LICA optical laboratory of the Universidad Complutense de Madrid using a monochromator, a calibrated photodiode and an integration sphere. The TCS 34725 has a Field of View that is very similar to a cosine function and is as such more sensitive in the axis perpendicular to the given cube's face. Aside from the light sensors, the LAN^3 contains a real-time clock, a micro-SD card to store the data, a GPS module and a temperature sensor. The raw Analog to Digital Units (ADU) recorded in each band along with the integration time and the gain are stored at each reading on the SD card along with the date, time, GPS coordinates, temperature and humidity (if available). The minimum light level detected is of the order of 0.005 lux. To get a better accuracy than 5%, we must restrict the measurement to light levels above 0.1 lux which correspond to a typical ADU of $\approx$20. The LAN^3 is equipped with an automated gain and integration time adjustment algorithm allowing the setup of optimal values that maximize the photometric resolution of each light sensor while keeping the integration time as low as possible (increasing the data acquisition rate). The LAN^3 in its first version (LAN^{3}v1) is based on the Arduino open source hardware so that it can be replicated by most people at low cost. All the required documentation to learn how to build the device is available online [19]. Figure 2a shows the LAN^{3}v1. A new version of the device (LAN^{3}v2) will be released soon. This version will have shorter acquisition time because it is able to simultaneously acquire all sensors and because we removed the bottom sensor. It is an important limitation of v1. The LAN^{3}v2 will allow the monitoring of its state along with a visual access to the data from a mobile device. The second version uses the Raspberry Pi computer instead of the Arduino microcontroller. In addition, the LAN^{3}v2 have an Uninterruptible Power Supply (UPS) to protect the system against power failures. A picture of LAN^{3}v2 is given in Figure 2b. The radiometric properties of the LAN^{3}v2 remain identical to LAN^{3}v1. A quick comparison of the differences between the v1 and v2 is available in Table 1.

Preprints (www.preprints.org) | NOT PEER-REVIEWED | Posted: 12 November 2020 doi:10.20944/preprints202011.0347.v1

Table 1. Features comparison of LAN^3 versions.

Feature	v1	v2
Sensors	TCS 34725	TCS 34725
Number of sensors	6	5
Minimum acquisition time	7 s	1 s
Maximum acquisition time	11 s	2 s
Processing unit	Arduino atMega 2560	Raspberry Pi 4b computer
Access to data	Removal of the microSD card	Download from wifi
System state indicator	RGB LED	RGB LED + wifi web server
Environment sensor	DTH22 (temp. and Hum.)	Onboard Raspberry pi temp. sensor
Power source	5 V - USB/A	5 V - USB/C
Power protection	Nothing	Integrated UPS
Positioning	GPS	GPS
Real time clock	DS 3231	DS 3231

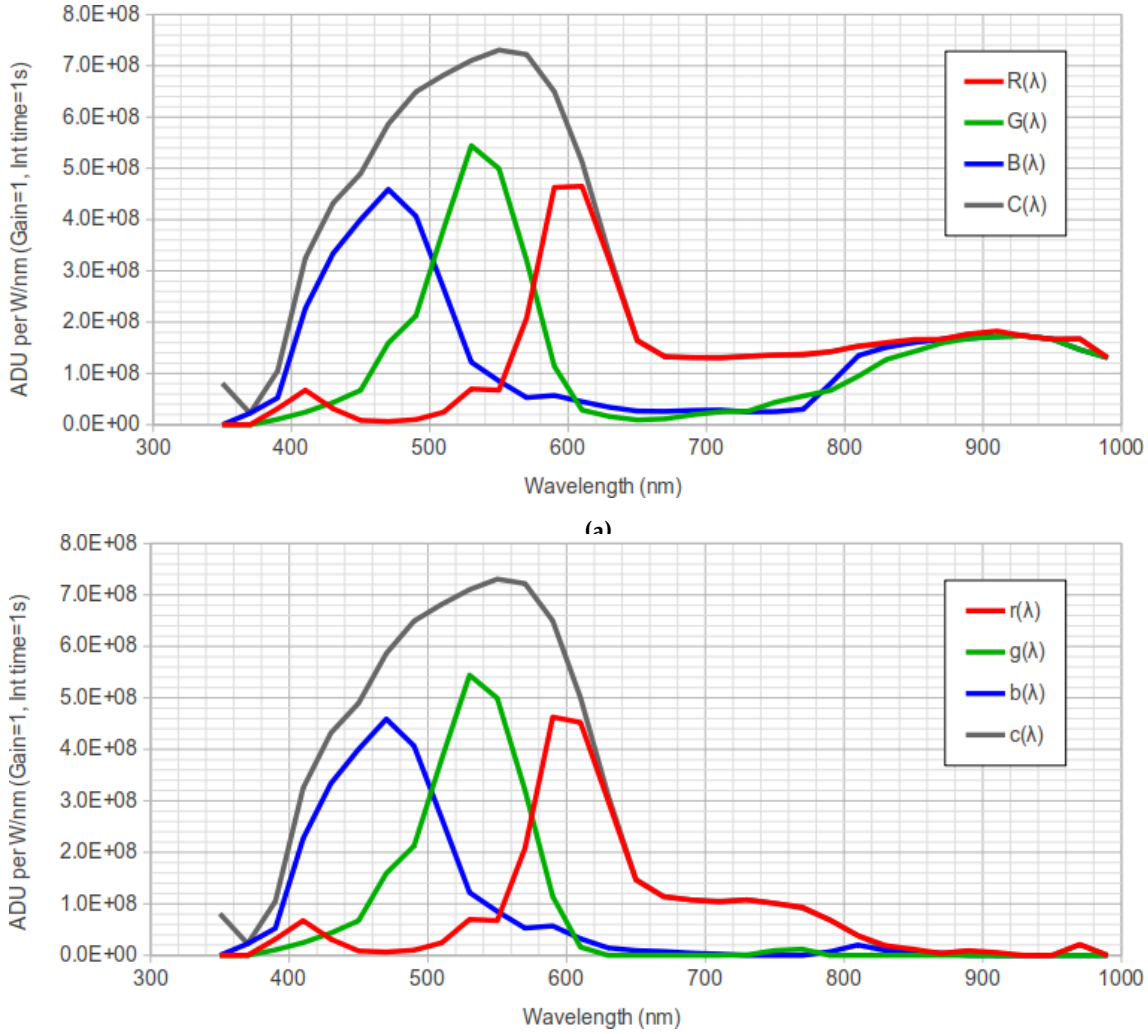

Figure 1. Spectral response $R(\lambda)$, $G(\lambda)$, $B(\lambda)$, and $C(\lambda)$ (Red, Green, Blue, Clear bands) of the LAN^3 as determined at the LICA laboratory at Universidad Complutense de Madrid. The calibration curves are for a gain of 1 and an integration time of 1s. In panel (b) we show $r(\lambda)$, $g(\lambda)$, $b(\lambda)$, and $c(\lambda)$ which are the band responses after removal of an estimate of the Infrared contribution (see Equations 1 and 2).

Preprints (www.preprints.org) | NOT PEER-REVIEWED | Posted: 12 November 2020 doi:10.20944/preprints202011.0347.v1

(a) v1 **(b)** v2

Figure 2. The LAN^3 devices.

2.2. Synthetic photometry

With the spectral responses of the sensor/glass window known, synthetic photometry can be used to simulate the signal that must be detected by the LAN^3 for any given spectrum. This is done by taking the weighted integral of the spectra over each of the sensors bands with the known spectral response of each band (see Figure 1a). To convert the RGBC response to rgbc. T, we removed an estimate of the infrared signal (IR) by using RGBC signals (see Figure 1b). The infrared spectral response can be computed using Equation 1.

$$IR(\lambda) \approx \frac{R(\lambda) + G(\lambda) + B(\lambda) - C(\lambda)}{2} \tag{1}$$

The resultant spectral sensitivity in the infrared ($IR(\lambda)$) is presented in Figure 3.
Therefore, $r(\lambda)$, $g(\lambda)$, $b(\lambda)$ and $c(\lambda)$ can be obtained with Equations 2.

$$r(\lambda) \approx R(\lambda) - IR(\lambda) \quad g(\lambda) \approx G(\lambda) - IR(\lambda) \quad b(\lambda) \approx B(\lambda) - IR(\lambda) \quad c(\lambda) \approx C(\lambda) - IR(\lambda) \tag{2}$$

Finally, the readings excluding the infrared are given by Equation 3.

$$r = \int J(\lambda)\, r(\lambda)\, d\lambda \qquad g = \int J(\lambda)\, g(\lambda)\, d\lambda \qquad b = \int J(\lambda)\, b(\lambda)\, d\lambda \qquad c = \int J(\lambda)\, c(\lambda)\, d\lambda \tag{3}$$

Where r, g, b and c are the simulated ADU values of the LAN^3 sensor excluding the infrared, when looking to a given light radiant flux. $J(\lambda)$ is the spectrum of the given light radiant flux and $r(\lambda)$, $g(\lambda)$, $b(\lambda)$ are respectively the spectral response of the Red, Green and Blue bands of the LAN^3 after removal of the infrared response.

In order to establish a relationship between LAN^3 measurements and MSI/SLI/IPI values, 314 different spectra were measured with a Sellarnet's Black comet spectrometer. The spectrometer operates in the spectral range 280-900 nm with a resolution of 1 nm. The sample set contains 172 street lights, indoor lamps and other types of conventional lighting commonly available. These spectra are coming from the Lamp Spectral Power Distribution Database (LSPDD, Roby *et al.* [20]). The remaining 142 spectra were acquired in situ. This allowed us to have mixed spectra combining multiple sources and environments. The wide variety of spectra is a key to establish a robust relationship over the colour

Preprints (www.preprints.org) | NOT PEER-REVIEWED | Posted: 12 November 2020 doi:10.20944/preprints202011.0347.v1

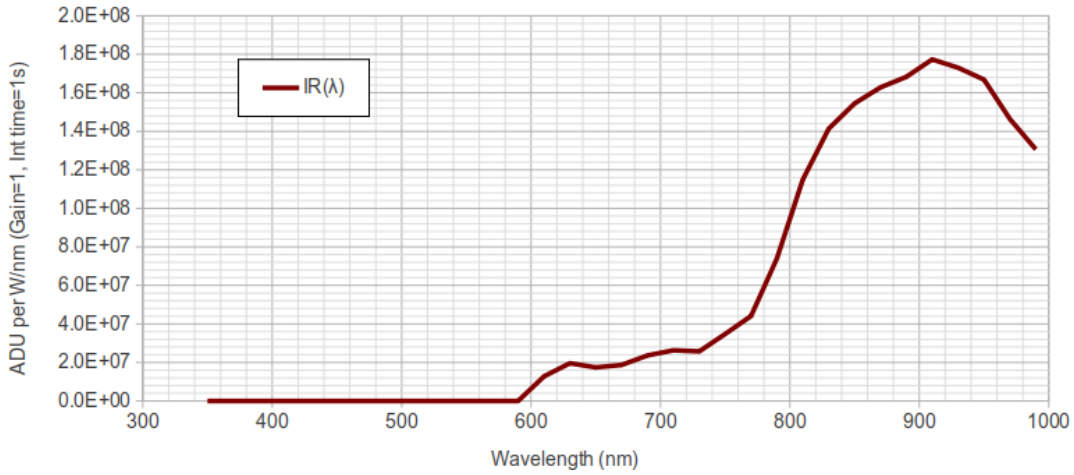

Figure 3. Estimated infrared spectral response.

ratios space defined by the $\left[\frac{b}{g}\right]$ and $\left[\frac{r}{g}\right]$. The r, g, and b values are the expected signals of the LAN[3] after removal of the infrared contribution to raw readings (see Equations 5 and 6.

2.3. Calculation of the indices from spectral data

The calculation of the MSI, the SLI and the IPI is done using the method described in Aubé *et al.* [13] over the LSPDD and in-situ spectra. The spectral responses used to calculate the indices come from Aubé *et al.* [13] for MSAS, Vos [21] for Scotopic ($V'(\lambda)$), DIN5031–10 [16] for PAS and Wyszecki and Stiles [22] for Photopic ($V(\lambda)$). These spectral responses can be downloaded from the LSPDD. The CIE standard illuminant D65 spectrum, also used in the indices calculations, was taken from the LSPDD.

2.4. Fitting the indices 3D surface in the $\left[\frac{b}{g}\right] - \left[\frac{r}{g}\right]$ *space*

Once the MSI, SLI, and IPI values are calculated with the spectra, they are compared with the LAN[3] colour ratios $\left[\frac{b}{g}\right]$ and $\left[\frac{r}{g}\right]$ of each spectrum as determined by the synthetic photometry method explained in section 2.2. This creates three 3D spaces, one for MSI (Figure 4), one for SLI and one for IPI, each one having 314 data points. For each 3D space, a 3D surface is fitted to the data and the equation 4 of this surface becomes the transformation equation between the LAN[3] colour ratios and the respective index value. The equation is the same for each index but the parameters α to ζ differ. The purpose of the division by the g value is to remove the effect of absolute luminous intensity on the radiometric measurements of the instrument. We used a Python code to fit a 2[nd] order polynomial 3D surface into the data for each index (see Equation 4).

$$Index = \alpha + \beta\left[\frac{b}{g}\right] + \gamma\left[\frac{r}{g}\right] + \delta\left[\frac{b}{g}\right]\left[\frac{r}{g}\right] + \epsilon\left[\frac{b}{g}\right]^2 + \zeta\left[\frac{r}{g}\right]^2 \quad (4)$$

3. Results

The method described above was applied to a large variety of spectral power distributions and indices. The results for MSI is presented in Figure 4. In that figure the light blue circles are the 314 spectra. The light blue transparent surface is the result of a fit of a 3D 2[nd] order polynomial surface to the whole dataset. At a first glance, it can be seen that the surface can relatively well capture the various points of the dataset and also that the sampling of the $\left[\frac{r}{g}\right]$ and $\left[\frac{b}{g}\right]$ space, while not perfect, is quite good. This actually indicates that a good variety of spectra was used. The fitted parameters of Equation 4 for each index are given in Table 2.

Preprints (www.preprints.org) | NOT PEER-REVIEWED | Posted: 12 November 2020 doi:10.20944/preprints202011.0347.v1

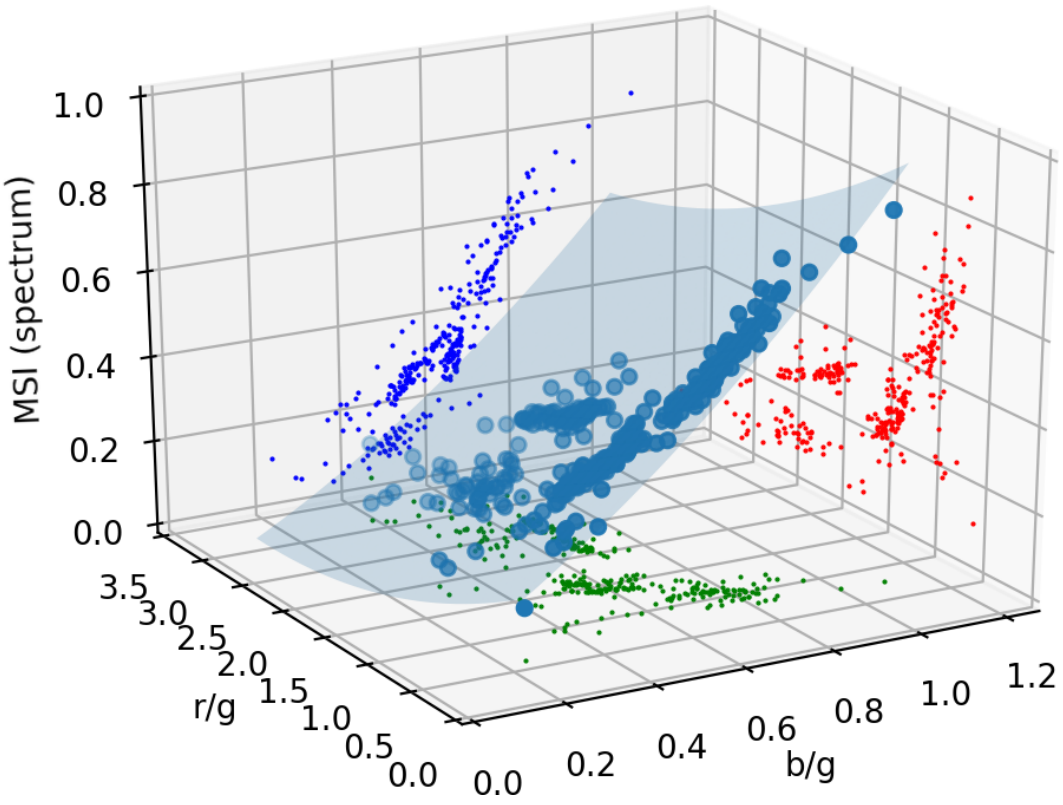

Figure 4. Fit of a second order polynomial surface for the Melatonin Suppression Index. The light blue circles are the 314 spectra. The r, g, b values are determined from synthetic photometry using the $r(\lambda)$, $g(\lambda)$ and $b(\lambda)$ spectral responses shown in Figure 1b. The dots are the projection of the point on each orthogonal plane (red = $\left[\frac{r}{g}\right]$ - MSI; green = $\left[\frac{b}{g}\right]$ - $\left[\frac{r}{g}\right]$; dark blue = $\left[\frac{b}{g}\right]$ - MSI)

Table 2. Fitted coefficients of equation 4 for the MSI, SLI and IPI.

Index	α	β	γ	δ	ϵ	ζ
MSI	0.0769	0.6023	-0.1736	-0.0489	0.3098	0.0257
SLI	0.6624	-0.4308	-0.2891	0.2913	0.6801	0.0015
IPI	-0.4118	-0.3824	-0.0955	0.7048	0.3305	-0.0463

Preprints (www.preprints.org) | NOT PEER-REVIEWED | Posted: 12 November 2020 doi:10.20944/preprints202011.0347.v1

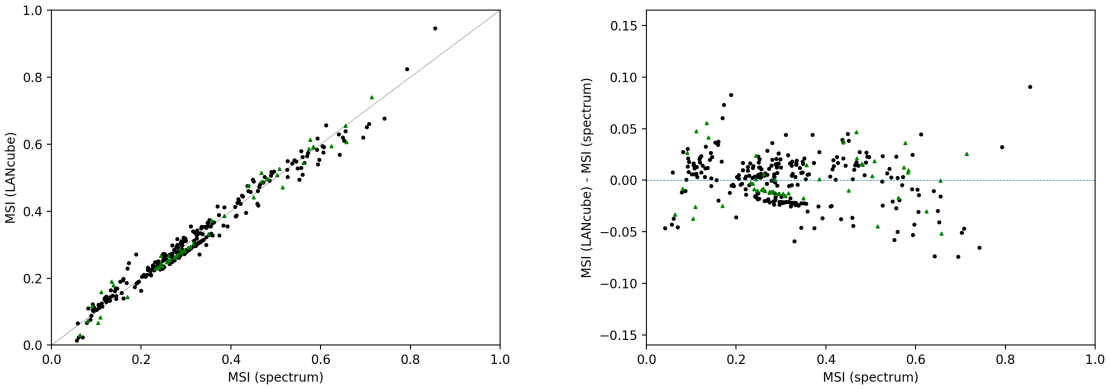

(a) **(b)**

Figure 5. Scatterogram of the LAN[3] derived MSI vs. MSI calculated with the spectrum. The black circles are derived from spectra of the LSPDD while the green triangles correspond to spectra sampled in the field.

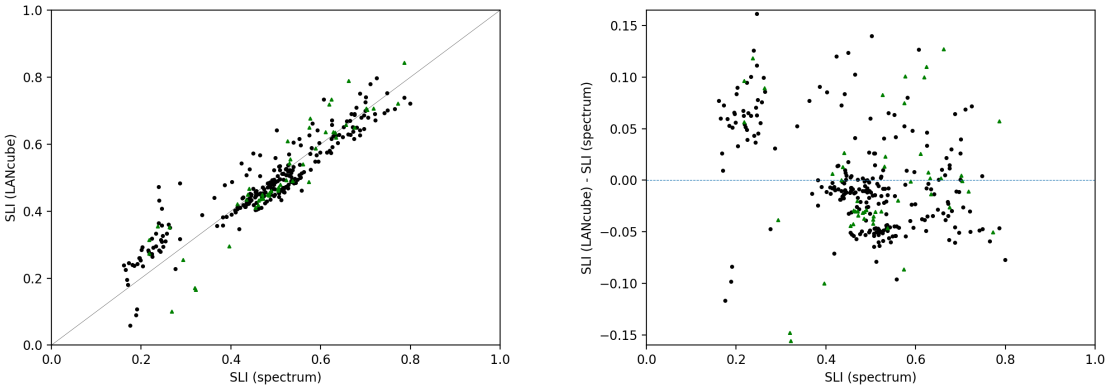

(a) **(b)**

Figure 6. Scatterogram of the LAN[3] derived SLI vs. SLI calculated with the spectrum. The black circles are derived from spectra of the LSPDD while the green triangles correspond to spectra sampled in the field.

For the three indices, the most important colour ratio is $\left[\frac{b}{g}\right]$ but nevertheless $\left[\frac{r}{g}\right]$ cannot be neglected at all. In the search for the optimal equation, we tried lower order polynomial functions but the results were not satisfying. In order to evaluate the intrinsic errors associated with the use of the fitted equations, we used them to calculate the three indices and compared the resultant indices to the accurate indices calculations obtained with the spectra. This is shown in Figures 5, 6 and 7. The figures show a good correlation between the two ways of determining the indices. In these figures, the solid line is the 1:1 relation and the right panel of each figure shows the residuals. For the MSI, the standard deviation of the residuals is 0.024 while it is 0.056 for the SLI. The correlation is a bit lower for the IPI where more points deviate more than 0.1 which reflect in a standard deviation of 0.107. Such standard deviations translate in the margin of error (95 percent confidence interval) of ± 0.05 for MSI, ± 0.1 for SLI, and ± 0.2 for IPI. Table 3 shows example results extracted from the 314 samples for different lamp technologies and CCT.

3.1. Maps of the MSI and SLI for Sherbrooke, Canada

As a direct result of the method that we developed, and to demonstrate the new possibility it delivers, we scanned the region of Sherbrooke City in Québec, Canada using the LAN[3] device installed

Preprints (www.preprints.org) | NOT PEER-REVIEWED | Posted: 12 November 2020 doi:10.20944/preprints202011.0347.v1

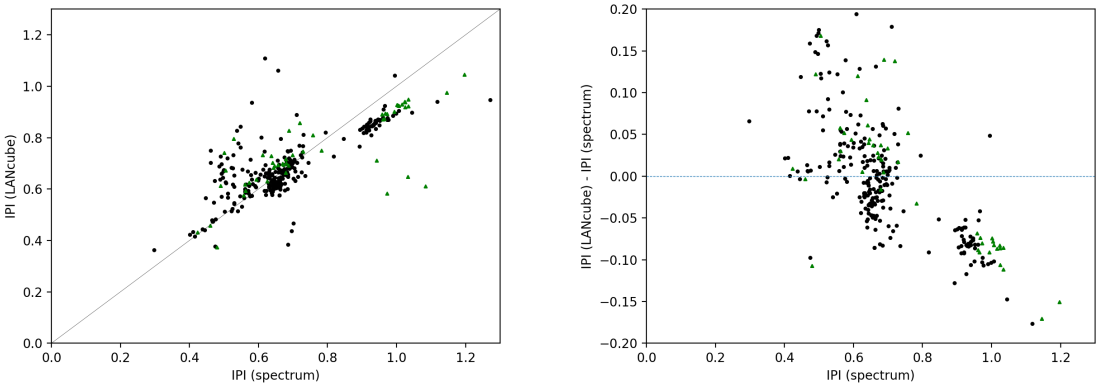

(a) **(b)**

Figure 7. Scatterogram of the LAN[3] derived IPI vs. IPI calculated with the spectrum. The black circles are derived from spectra of the LSPDD while the green triangles correspond to spectra sampled in the field.

Table 3. Examples of colour ratios and indices for different technologies and CCT.

Technology	CCT	$\frac{b}{g}$	$\frac{r}{g}$	MSI	SLI	IPI
	K	-	-	-	-	-
HPS	2000	0.49	2.11	0.12	0.24	0.51
Metal Halide	4000	0.80	0.93	0.56	0.70	0.66
LED	1800	0.39	2.97	0.06	0.19	0.7
LED	2500	0.51	1.58	0.21	0.41	0.66
LED	2700	0.54	1.47	0.25	0.44	0.66
LED	3000	0.57	1.32	0.29	0.49	0.65
LED	3500	0.56	1.17	0.32	0.50	0.64
LED	4000	0.77	0.95	0.56	0.62	0.62
LED	5000	0.75	0.80	0.60	0.66	0.66
CFL	2700	0.47	1.38	0.21	0.41	0.53
CFL	3000	0.54	1.33	0.27	0.45	0.56
CFL	4100	0.77	0.95	0.54	0.67	0.66
CFL	5000	0.78	0.86	0.57	0.72	0.67
CFL	6400	0.81	0.70	0.64	0.80	0.66
Fluorescent	4000	0.61	0.97	0.37	0.59	0.57
Incandescent	2300	0.62	2.93	0.19	0.42	1.04
Halogen	3000	0.65	2.02	0.31	0.52	0.93

Preprints (www.preprints.org) | NOT PEER-REVIEWED | Posted: 12 November 2020 doi:10.20944/preprints202011.0347.v1

on top of a car. The cube was aligned parallel to the moving direction and only the lateral sensors (toward houses) were used. This allows to form a better idea on the light pollution that can enter bedrooms and potentially impact human health. We drove the city with such installation. The r, g, b are calculated with data R, G, B, C data collected with the LAN^3 using Equations 5, 6 and 7.

$$IR \approx \frac{R' + G' + B' - C'}{2} \tag{5}$$

$$r \approx R' - IR \qquad g \approx G' - IR \qquad b \approx B' - IR \tag{6}$$

With

$$R' = R/A/t_i \qquad G' = G/A/t_i \qquad B' = B/A/t_i \tag{7}$$

where A and t_i are respectively the sensor gain and the integration time (s) recorded by the LAN^3. Note that in Equation 7, t_i is expressed in seconds while the LAN^3 is recording it in units of milliseconds. The recorded values have to be divided by 1000 prior to using Equation 7. In general, it is better to make the correction because the spectral response curves of Figure 1a were determined for $gain = 1$ and $t_i = 1$s. But in the present study, it is not mandatory because that for a given sensor, the gain and integration time are the same for all bands and then taking the bands ratios cancel their effect. In the LAN^3, the gain varies from 1 to 60 and the integration time from 2.4 to 614 ms depending on the ambient light level.

The $\left[\frac{b}{g}\right]$ and $\left[\frac{r}{g}\right]$ values were converted into MSI, SLI and IPI values using Equation 4. We excluded extrapolated data that are outside the span of values of data used for the fit. This was done by excluding indices lower than zero and higher than two. During the calculation of an index, all recorded R, G, B, C values are subject to a threshold value set at 20. Such a threshold value ensure that the Signal to Noise Ratio (SNR) is higher than 20 (i.e., noise represents less than 5% of the signal). In order to generate the maps from the localized measurements, we used the nearest neighbour interpolation with a maximum interpolation distance of 30 m. The resulting maps are shown in Figures 8, 9, and 10. The relation between the lighting technologies and the map index classes are given in Tables 4, 5, and 6.

Preprints (www.preprints.org) | NOT PEER-REVIEWED | Posted: 12 November 2020 doi:10.20944/preprints202011.0347.v1

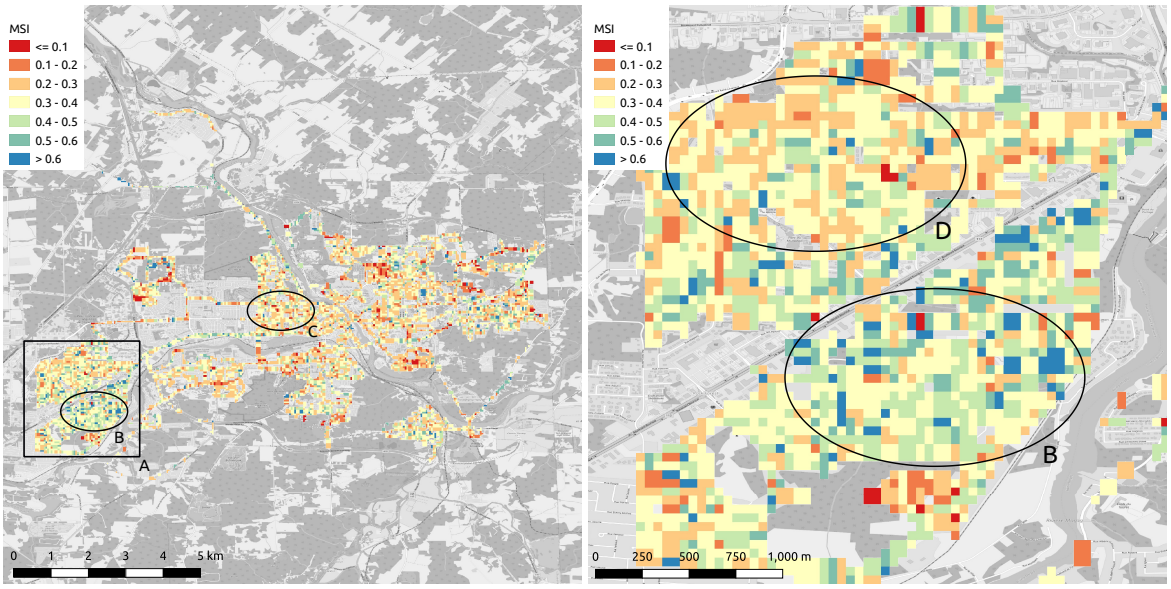

(a) **(b)**

Figure 8. Map of the MSI for Sherbrooke, Canada. We used Equation 4 and Table 2 with LAN^3 data. The panel (b) shows a zoomed view of MSI for the Mi-Vallon sector of Sherbrooke, Canada (black square A in panel (a)).

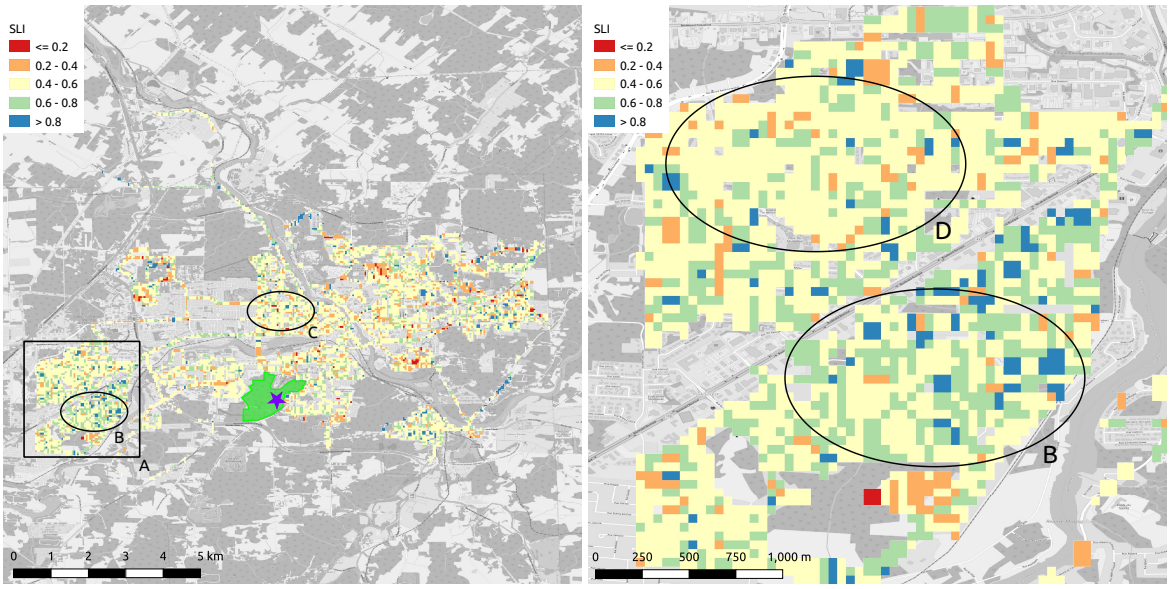

(a) **(b)**

Figure 9. Same as Figure 8 but for the SLI index. The purple star is the epicentre of the Urban Dark Sky Oasis and the green polygon correspond to the limits of the protected area.

Preprints (www.preprints.org) | NOT PEER-REVIEWED | Posted: 12 November 2020 doi:10.20944/preprints202011.0347.v1

Table 4. Lamps associated to mapped MSI ranges determined with the LSPDD. CFL stands for Compact Fluorescent, FL for fluorescent, WW for warm white, NW for neutral white, CW for cool white.

MSI range	Lamp spectra
[0.0, 0.1[	LED PCamber, Yellow CFL, Red CFL
[0.1, 0.2[	LED 2500K, Incandescent, HPS
[0.2, 0.3[	LED 2700K, LED 3000K, Incandescent, WW CFL
[0.3, 0.4[	LED 3000K, Incandescent, Halogene, WW CFL
[0.4, 0.5[	LED 4000K, NW CFL, NW FL
[0.5, 0.6[	LED 5000K, NW CFL, MH
[0.6, 0.7[	LED 5000K, NW CFL, CW CFL, MH
[0.7, 0.8[	LED 6000K, CW CFL
[0.8, 0.9[	-
[0.9, 1.0[	Blue CFL, Blue LED

Table 5. Lamps associated to mapped SLI ranges determined with the LSPDD. CFL stands for Compact Fluorescent, FL for fluorescent, WW for warm white, NW for neutral white, CW for cool white.

SLI range	Lamp spectra
[0.0, 0.1[	Red CFL
[0.1, 0.2[	PC amber LED
[0.2, 0.3[	HPS, Yellow CFL
[0.3, 0.4[	WW CFL, LED 2500K
[0.4, 0.5[	LED 2700K, LED 3000K, WW CFL Inc
[0.5, 0.6[	LED 4000K, Halogene, Incandescent
[0.6, 0.7[	LED 4000K, LED 5000K, NW CFL, NW FL, Halogene, MH
[0.7, 0.8[	LED 5000K, LED 6000K, CW CFL
[0.8, 0.9[	CW CFL
[0.9, 1.0[	Blue CFL, LED 6500K

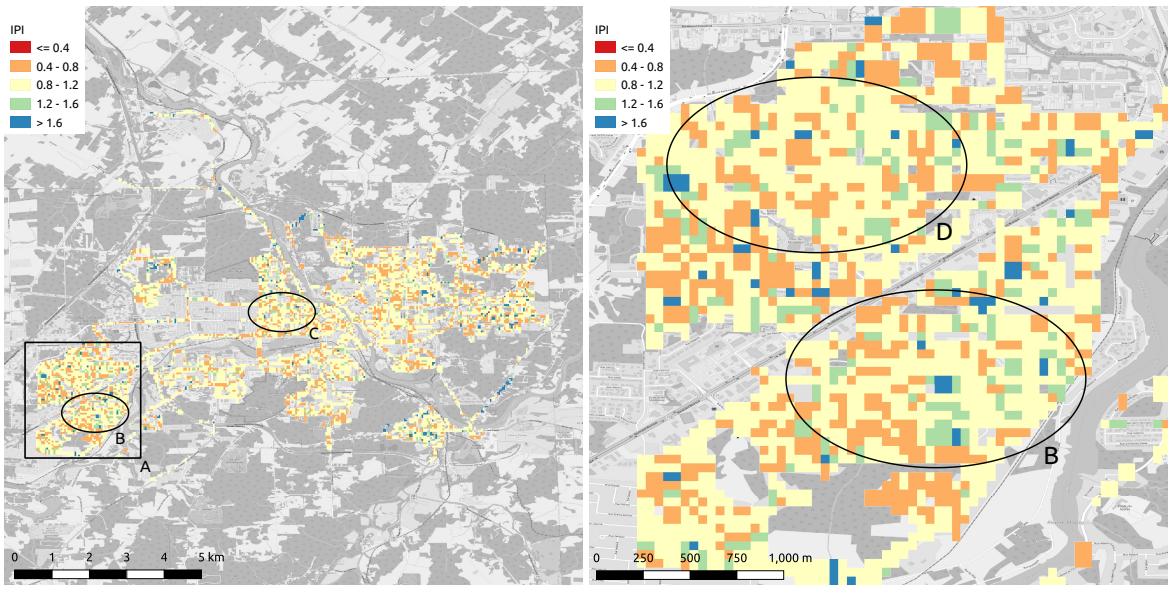

(a) **(b)**

Figure 10. Same as Figure 8 but for the IPI index.

4. Discussion and conclusion

We estimate that the equations found to convert the r, g, b values of the LAN[3] into the three spectral indices MSI, SLI and IPI are suited for the mapping of large territories. The margin of error (95 percent confidence interval) are ± 0.05 for the MSI, ± 0.1 for the SLI, and ± 0.2 for the IPI. The margin of error for MSI appears to be sufficiently small for many health and ecosystems studies. For the SLI

 doi:10.20944/preprints202011.0347.v1

Table 6. Lamps associated to mapped IPI ranges determined with the LSPDD. CFL stands for Compact Fluorescent, FL for fluorescent, WW for warm white, NW for neutral white, CW for cool white.

IPI range	Lamp spectra
$[0.0, 0.1[$	-
$[0.1, 0.2[$	-
$[0.2, 0.3[$	-
$[0.3, 0.4[$	-
$[0.4, 0.5[$	Yellow CFL
$[0.5, 0.6[$	HPS, WW CFL, PC amber LED
$[0.6, 0.7[$	WW CFL, NW CFL, LED 2700K, LED 3000K, LED 4000K
$[0.7, 0.8[$	NW CFL, CW CFL, LED 3000K, LED 4000K
$[0.8, 0.9[$	Halogene
$[0.9, 1.0[$	Halogene, Incandescent, Blue CFL, Red CFL

the margin of error is larger but it is still useful as a tool for night sky protection. Tables 4 and 5 show that the margins of errors associated with the MSI and the SLI are small enough to separate the type of light technologies in regard to their spectral content. So we should expect the maps produced to be precise enough for most applications. The margin of error is much larger for the IPI and therefore we think this index requires further analysis in order to find better suited colour ratios to establish a better index calculation formula.

The index maps show that the averaged value all over the city for the MSI, the SLI and the IPI are 0.34, 0.54 and 0.96 respectively. Such numbers can be used to estimate a city performance to protect its territory against related issues. As an example, for the MSI, the average value is relatively small (0.34). As an element of comparison, this value is typical of 3000K lamps. However, since the sensor detects all light emissions, this value is the result of a combination of both public and private lights. The sensitivity to private lights is probably higher given that we are using the lateral sensors and in Sherbrooke private lights are generally installed at a lower height. In the city of Sherbrooke, the street lights are mainly composed of High-Pressure Sodium (HPS) (MSI $\approx$ 0.12, [13]) and PC Amber LEDs (MSI $\approx$ 0.04, [13]).

The indices maps allow us to identify critical zone in terms of their expected potential impact. As an example, Figure 8 shows only few values above MSI=0.6 in the city of Sherbrooke (blue points in Figure 8a). Such data correspond to critical locations with respect to their potential impact on the melatonin suppression. In Sherbrooke, many of them are located in the main commercial zones. The residential Mi-Vallon sector is an exception (square A of Figure 8a and Figure 8b for a zoomed-in view). The peculiarity of that residential area is clear when comparing zone B and zone C in Figure 8a. Zone C presents lower values of MSI but both zones are residential. In the Mi-Vallon sector, we can even distinguish two regimes between the northern (zone D in Figure 8b) and southern zones (zone B in Figure 8b). Zone B showing a much higher occurrence of high MSI values, but both zones are residential. They actually differ mainly by their date of construction, zone D being the most recent. Lower MSI values in zone D actually reflect that the city administration is now gradually installing/converting street lights to PC amber, but another reason for such difference is that more houses are equipped with front door white bulbs in zone B than in zone D. Such private lamps are potential threat to the citizen's health, but as they are under the control of the citizens themselves, it highlights the need for public outreach measures. Fortunately, we can find many places with very low MSI (<0.1) in the city. This situation happens because of the new city policy to replace or install street lights by using PC amber LEDs and sometimes 2200K LEDs along with the absence of white private lamps.

A similar analysis can be made for the SLI and IPI index with Figures 9 and 10 respectively. One should keep in mind that the margin of error for SLI is twice the one of MSI and that IPI margin of error is a 4-fold of the MSI. In the case of SLI, the blue pixel correspond to SLI higher than 0.8. These places are the one to consider first when it's time to restore the starry sky. Such information is highly

strategic in the case of Sherbrooke because of the current project undergoing to create an Urban Dark Sky Oasis. This project aims to give access to the Milky Way to the citizens in the Mont Bellevue city park. The limits of the park are identified by a green polygon in Figure 9a.

The mapping method presented here is a way to rapidly identify the potentially harmful installations and then prepare targeted interventions to reduce or eliminate the problem. In a future work, we plan to find empirical relationships between the RGB and illuminance (lux) and the Correlated Colour Temperature (CCT). One other improvement could be to search for better set of colour ratios, including the clear channel, that could increase the correlation between the fitted equation and the MSI, the SLI and the IPI established with spectral data. This later task would be particularly useful for the IPI index given its large associated margin of error.

Author Contributions: We applied the sequence-determines-credit approach [23] for the sequence of authors which is in order of decreasing contributions. Conceptualization, M.A. and J.R.; methodology, M.A. and C.M.; software, M.A. C.M.; validation, M.A., C.M., A.D. and A.F.; formal analysis, M.A., C.M., A.F., A.D., A.S., J.Z. and C.T.; investigation, M.A., C.M., J.Z., C.T., A.F. and A.D.; resources, M.A.; data curation, C.M. and M.A.; writing–original draft preparation, M.A., A.F., A.D. and C.M.; writing–review and editing, M.A., C.M., A.F., A.D., J.R., J.Z., A.S. and C.T.; visualization, C.M., M.A. and A.S.; supervision, M.A., J.R. and C.M.; project administration, M.A.; funding acquisition, M.A. and J.R.

Funding: M. A., A. F. and C. M. thanks the Fonds de recherche du Québec – Nature et technologies (FRQNT) for financial support through the Research program for college researchers. J. R., M. A., A. F. and A. D. thank the Pôle régional en enseignement supérieur de l'Estrie (PRESE).

Acknowledgments: We want to thank, Thomas Goulet-Soucy for his contribution to the design of the prototype version of the LAN^3. We also want to thank Elsa Vigneau, Mathieu Fréchette and Thomas Goulet-Soucy for their help during the initial LAN^3 testing and calibration experiments in Barcelona, Madrid, Lyon and Toulouse. Finally, we want to thank DH éclairage Inc. who built and graciously provided us the LAN^{3}v1 systems used to map the city of Sherbrooke.

Conflicts of Interest: The authors declare no conflict of interest.

Abbreviations

The following abbreviations are used in this manuscript:

ADU	Analog to Digital Unit
ALAN	Artificial Light at Night
CFL	Compact fluorescent
CIE	Commission Internationale de l'Éclairage
DALAN	Direct Artificial Light at Night
DSLR	Digital single-lens reflex camera
FRQNT	Fonds de recherche du Québec – Nature et technologies
GPS	Global Positioning System
HPS	High-Pressure Sodium
IPI	Induced Photosynthesis Index
LED	Light Emitting Diode
LSPDD	Lamp Spectral Power Distribution Database
MSAS	Melatonin Suppression Action Spectrum
MSI	Melatonin Suppression Index
nm	nanometre
PAS	Photosynthesis Action Spectrum
PC	Phosphor Converted
PRESE	Pôle régional en enseignement supérieur de l'Estrie
SLI	Star Light Index
SNR	Signal to Noise Ratio
UPS	Uninterruptible Power Supply

References

1. Gaston, K.J.; Visser, M.E.; Hölker, F. The biological impacts of artificial light at night: the research challenge. *Philosophical Transactions of the Royal Society B* **2015**, *370*, 20140133.
2. Russart, K.L.G.; Nelson, R.J. Artificial light at night alters behavior in laboratory and wild animals. *Journal of Experimental Zoology Part A: Ecological and Integrative Physiology* **2018**, *329*, 401–408.
3. Briggs, W.R. Physiology of plant responses to artificial lighting. *Ecological Consequences of Artificial Night Lighting* **2006**, pp. 389–411.
4. Riegel, K.W. Light pollution: outdoor lighting is a growing threat to astronomy. *Science* **1973**, *179*, 1285–1291.
5. Cho, Y.; Ryu, S.H.; Lee, B.R.; Kim, K.H.; Lee, E.; Choi, J. Effects of artificial light at night on human health: a literature review of observational and experimental studies applied to exposure assessment. *Chronobiology International* **2015**, *39*, 1294–1310.
6. Duffy, J.F.; Wright Jr, K.P. Entrainment of the human circadian system by light. *Journal of Biological Rhythms* **2005**, *20*, 326–338.
7. Evans, J.A.; Davidson, A.J. Health consequences of circadian disruption in humans and animal models. *Progress in Molecular Biology and Translational Science* **2013**, *119*, 283–323.
8. Lockley, S.W.; C., B.G.; A., C.C. High sensitivity of the human circadian melatonin rhythm to resetting by short wavelength light. *The Journal of Clinical Endocrinology & Metabolism* **2003**, *88*, 4502–4505.
9. Brainard, G.C.; Hanifin, J.P.; Greeson, J.M.; Byrne, B.; Glickman, G.; Gerner, E.; Rollag, M.D. Action spectrum for melatonin regulation in humans: evidence for a novel circadian photoreceptor. *Journal of Neuroscience* **2001**, *21*, 6405–6412.
10. Garcia-Saenz, A.; Sánchez de Miguel, A.; Espinosa, A.; Costas, L.; Aragonés, N.; Tonne, C.; Moreno, V.; Pérez-Gómez, B.; Valentin, A.; Pollán, M.; Castaño-Vinyals, G.; Aubé, M.; Kogevinas, M. Association Between Outdoor Light-at-night Exposure and Colorectal Cancer in Spain. *Epidemiology* **2020**, *31*, 718–727.
11. Garcia-Saenz, A.; Sánchez de Miguel, A.; Espinosa, A.; Valentin, A.; Aragonés, N.; Llorca, J.; Amiano, P.; Sánchez, M.; Vicente, G.; Marcela, C.; Rocío.; Aubé, M.; others. Evaluating the association between artificial light-at-night exposure and breast and prostate cancer risk in Spain (MCC-Spain study). *Environmental health perspectives* **2018**, *126*, 047011.
12. Rybnikova, N.; Portnov, B.A. Population-level study links short-wavelength nighttime illumination with breast cancer incidence in a major metropolitan area. *Chronobiology international* **2018**, *35*, 1198–1208.
13. Aubé, M.; Roby, J.; Kocifaj, M. Evaluating potential spectral impacts of various artificial lights on melatonin suppression, photosynthesis, and star visibility. *PloS one* **2013**, *8*, e67798.
14. Thapan, K.; Arendt, J.; Skene, D.J. An action spectrum for melatonin suppression: evidence for a novel non-rod, non-cone photoreceptor system in humans. *The Journal of physiology* **2001**, *535*, 261–267.
15. Brown, R.L.; Robinson, P.R. Melanopsin—shedding light on the elusive circadian photopigment. *Chronobiology international* **2004**, *21*, 189–204.
16. DIN5031–10. Optical radiation physics and illuminating engineering - Part 10: Photobiologically effective radiation, quantities, symbols and action spectra., 2000.
17. Sánchez de Miguel, A.; Bará, S.; Aubé, M.; Cardiel, N.; Tapia, C.E.; Zamorano, J.; Gaston, K.J. Evaluating human photoreceptoral inputs from night-time lights using RGB imaging photometry. *Journal of Imaging* **2019**, *5*, 49.
18. Sánchez de Miguel, A.; Kyba, C.C.; Aubé, M.; Zamorano, J.; Cardiel, N.; Tapia, C.; Bennie, J.; Gaston, K.J. Colour remote sensing of the impact of artificial light at night (I): The potential of the International Space Station and other DSLR-based platforms. *Remote sensing of environment* **2019**, *224*, 92–103.
19. Aubé, Martin. LANcube webpage., 2020. https://lx02.cegepsherbrooke.qc.ca/ aubema/index.php/Prof/LANcube.
20. Roby, J.; Aubé, M.; Morin Paulhus, A. LSPDD: Lamp Spectral Power Distribution Database, 2017. http://lspdd.com.
21. Vos, J.J. Colorimetric and photometric properties of a 2° fundamental observer. *Color Research & Application* **1978**, *3*, 125–128.
22. Wyszecki, G.; Stiles, W.S. *Color science*; Vol. 8, Wiley New York, 1982.

 doi:10.20944/preprints202011.0347.v1

23. Tscharntke, T.; Hochberg, M.E.; Rand, T.A.; Resh, V.H.; Krauss, J. Author sequence and credit for contributions in multiauthored publications. *PLoS biology* **2007**, *5*, e18.